Electron Transfer between Quinones in Photosynthetic Reaction Centers

Mariangela Di Donato,[†] Andrea Peluso,*[,†] and Giovanni Villani[‡]

Dipartimento di Chimica, Università di Salerno, I-84081 Baronissi, Salerno, Italy,and Istituto per i Processi Chimico Fisici, IPCF, CNR, via G. Moruzzi 1, I-56124, Pisa, Italy

Received: September 8, 2003; In Final Form: January 7, 2004

The mechanism of electron transfer (ET) from the primary to the secondary quinone of bacterial photosynthetic reaction centers is discussed on the basis of theoretical computations of the minimum energy nuclear configurations and ET coupling elements, and quantum dynamic simulations of elementary reaction steps. For ET to occur via tunneling, unreasonably high values of the electronic coupling elements or very stringent energy conditions, i.e., tight degeneracy (within a few cm^{-1}) between the initial and final vibronic states, are necessary, both for the direct and through-bridge (superexchange) routes. The assumption of tight degeneracy significantly slows down the process so that other competitive processes, such as proton transfer from the H-bonded HisM219 to the primary quinone, can take place. All these results suggest that the iron−histidine bridge can play an important role in the ET mechanism.

Introduction

Photosynthesis is the process by which bacteria and plants photochemically convert low-energy substrates, such as water and carbon dioxide, into chemicals of high free-energy content.[1] The strategy adopted by living organisms to perform such an energy transduction is quite complex; the absorbed radiation energy is initially converted in electrostatic energy by promoting a sequence of photoinduced electron transfers (ET), leading to a charge-separated state in a a highly structured membrane.[2,3] The electric field is then used to transfer protons through the membrane in order to establish an electrochemical gradient across it, which, according to Mitchell's mechanism,[4] triggers the chemical reactions by which ATP and other biological fuels are produced.

The heart of such a molecular machinery is the photosynthetic reaction center (RC), a protein complex in which the sequence of long-range photoinduced ET takes place. The determination of the crystal structure of RCs from two purple photosynthetic bacteria, *Rhodopseudomonas viridis*[5,6] and *Rhodobacter sphaeroides*,[7,8] schematized in Figure 1, and of the light induced structural changes of the latter,[9] has opened the way toward the comprehension of the structure−function relationships that control the formation of photoinduced charge-separated states.

In bacterial RCs, the redox cycle leading to transmembrane charge separation starts from the absorption of a photon by a bacteriochlorophyll special pair (P),[10−13] which, from its excited singlet (P*), releases an electron to H, probably via the interposed BC.[14−16] The electron is transferred from P* to H, $\Delta G = 0.16$ eV,[17] and from the latter to Q_A, $\Delta G = 0.69$ eV,[18] on the picosecond time scale, 4 and 200 ps, respectively.[15,19−23] The next step consists of the reduction of the special pair by cytochrome c, followed by ET from Q_A to Q_B, ($\Delta G = 0.07$ eV).[18] The last two processes are comparatively much slower than previous ones; the reduction of P by cytochrome c takes place in ca. 270 ns,[22] whereas ET from Q_A to Q_B requires ca. 200 μs for the transfer of the first electron and 1 ms for the second one.[24] For an excellent review dealing with the early ET and proton transfer (PT) steps of photosynthesis, see ref 2.

The detailed knowledge of the mechanisms by which photoinduced charge-separated states are obtained in RCs of bacteria and plants, with an efficiency close to unity, is an important starting point for the rational design and realization of biomimetic synthetic systems for artificial photosynthesis.[25−27] In this paper, we intend to give a contribution to that field by focusing attention on the mechanism of the ET between quinones in bacterial RCs.

The mechanism of ET between quinones is the most interesting one. In fact, the slow rate of this process and the very long lifetime of the charge-separated state suggest that a chemical change involving the amino acidic residues surrounding ET cofactors, i.e., conformational gating[28−30] and proton-coupled electron transfer,[31−34] is expected to play a role. In line with that expectation, Graige et al. have shown that the ET rate from Q_A^- to Q_B does not change as the free energy of the reaction is changed; since the strong temperature dependence rules out the possibility that ET is activationless, it was suggested that the rate-determining step for ET from Q_A to Q_B is a conformational change of the protein.[28] From the comparison of the X-ray structures obtained in the dark and under illumination, that change has been identified with the large displacement of Q_B from the so-called distal site (Q_{B1}), a site in which Q_B is not H bonded to any of the histidines of the nonhaem iron complex interposed between Q_A and Q_B, to the proximal site (Q_{B2}), where Q_B is connected to Q_A by a H-bond chain, involving two opposite histidine residues coordinated to the iron ion.[9] However, recent FTIR measurements provide evidence that even when crystallized in the dark Q_B is prevalently in the proximal site;[35,36] moreover, the movement of Q_B from the distal to the proximal site cannot explain another important aspect of the early ET steps in RCs: the slowness of the backward charge-recombination process.

The slow rate of the charge-recombination process is a crucial point for an efficient conversion of the solar energy into chemical energy. In fact, the $P^+Q_A^-$ charge-separated state must

* Author to whom correspondence may be addressed. E-mail: apeluso@unisa.it.
[†] Università di Salerno.
[‡] Istituto per i Processi Chimico Fisici.

10.1021/jp036678t CCC: $27.50
Published on Web 02/05/2004

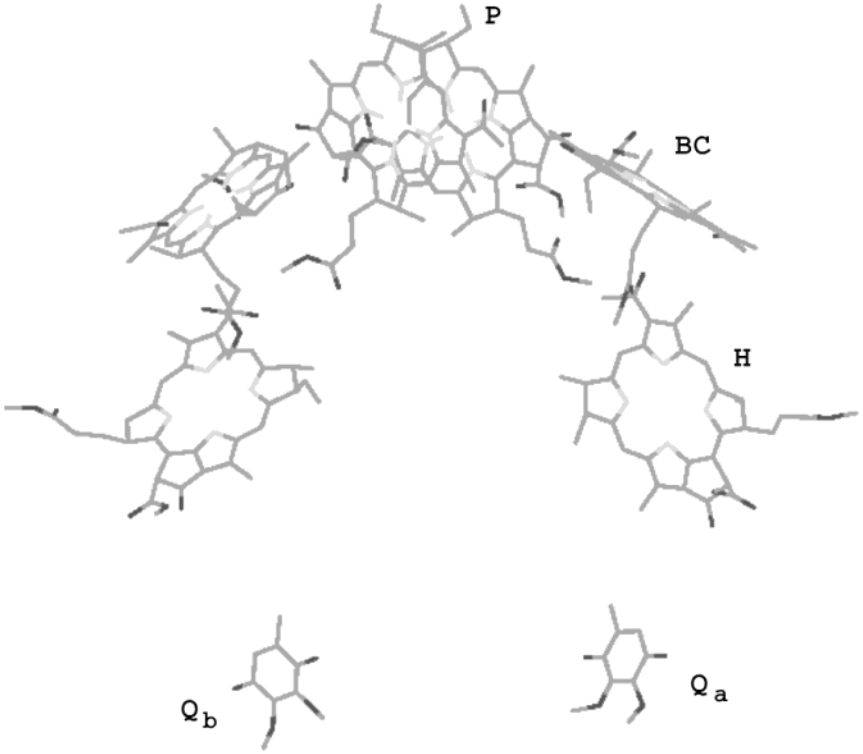

Figure 1. Schematic view of bacterial photosynthetic RC showing the main electron-transfer cofactors.

live long enough for the reduction of P^+ by cytochrome c to occur, and that cannot be explained by conformational changes involving only Q_B. Kinetic studies have provided evidence in favor of a temperature-dependent extra stabilization of the $P^+Q_A^-$ state, which can be due either to solvent reorganization, there is evidence of conformational changes on the microsecond time scale which may solvate Q_A^-,[29,30] or possibly to some chemical modification at Q_A site, probably involving proton movements around Q_A, as suggested by the broad positive band at 2900−2500 cm^{-1}, shifting at 2200−1800 cm^{-1} upon deuteration, observed in the Q_A^-/Q_A FTIR difference spectrum of photosynthetic RCs, both from *Rb. sphaeroides* and from *Rp. viridis*.[37]

Theoretical computations also suggest that the arrival of an electron on Q_A can lead to significant proton rearrangements around this site.[38−40] Ab initio computations predict that, upon reduction, the semiquinone anion takes up a proton from the H-bonded iron−histidine, delocalizing the negative charge (not the additional electron) on the positively charged iron−histidine bridge. ET from Q_B can then occur by shifting two hydrogen atoms, as in the long-range proton-assisted electron-transfer (PAET) mechanism.[31,32] An attractive feature of the PAET mechanism is that the first proton transfer step could be the chemical process that stabilizes the charge-separated state, increasing its lifetime. Experimental evidence has in fact shown that, in carotenoid-porphyrin-quinone triads exhibiting photoinduced ET, the addition of a carboxylic group, in a position in which it can form an intramolecular H-bond with a quinone oxygen, significantly stabilizes the charge-separated state, probably by transferring a proton from the carboxylic group to the semiquinone anion.[41]

Another interesting experimental finding is provided by the ENDOR spectra of the primary ubiquinone radical in frozen Zn-substituted RCs from *Rhodobacter sphaeroides*.[42] The ENDOR spectra of Q_A^- have shown a strong coupling with the N−H proton of HisM219, from which a very short O_4−H distance, 1.5−1.4 Å, was predicted.

There are therefore several experimental and theoretical pieces of evidence that point toward the assignment of an active role to the iron−histidine bridge in the mechanism of ET from Q_A^- to Q_B. However, before claiming the necessity of invoking alternative ET mechanisms, a study of the dynamical features of through-space mechanisms, such as tunneling and superexchange, is in order. In this paper, we report such a study, with the aim of comparing the efficiency and rates of these mechanisms with that of the alternative PAET mechanism,[39] of understanding what chemical and physical factors could distinguish different mechanisms, and hopefully of providing new hints and suggestions for guiding future experimental work.

ET Dynamics in Photosynthetic RCs

Model Hamiltonians. In the case of direct tunneling, we assume that there are only two low-lying diabatic electronic states, with the unpaired electron fully localized either on Q_A ($|A\rangle$) or Q_B ($|B\rangle$). The total Hamiltonian is then[43]

$$\mathscr{H} = |A\rangle[T_N + U_A]\langle A| + |B\rangle[T_N + U_B]\langle B| + |A\rangle \mathscr{V}'_{AB}\langle B| + c.c \quad (1)$$

where T_N is the nuclear kinetic energy operator, U is the electronic potential energy operator, and $\mathscr{V}'_{AB}$ is the electronic coupling between the two diabatic states

$$U_X = \langle X|\mathscr{H}^{el}|X\rangle \qquad X = A, B \quad (2)$$

$$\mathscr{V}'_{AB} = \langle A|\mathscr{H}^{el}|B\rangle \quad (3)$$

The total time-dependent vibronic wave function is expanded over a set of Born−Oppenheimer product wave functions

$$\Phi(t) = \sum_{\bar{v},w} \boldsymbol{C}_{A\bar{v}w}(t)|A\rangle|\bar{v}w\rangle + \sum_{\bar{v},w} \boldsymbol{C}_{B\bar{v}\bar{w}}(t)|B\rangle|v, \bar{w}\rangle, \quad (4)$$

where v and w denote the whole set of vibrational quantum

numbers associated to normal modes of Q_A (q_1) and Q_B (q_2) and the bar distinguishes quantities of the semiquinone anion. The expansion coefficients are determined by solving the time dependent Schrödinger equation

$$-i\hbar\begin{pmatrix}\dot{\boldsymbol{C}}_{A\bar{v}w}(t)\\ \dot{\boldsymbol{C}}_{B\upsilon\bar{w}}(t)\end{pmatrix}=\begin{pmatrix}\boldsymbol{H}_A & \boldsymbol{H}_{AB}\\ \boldsymbol{H}_{BA}^{\dagger} & \boldsymbol{H}_B\end{pmatrix}\begin{pmatrix}\boldsymbol{C}_{A\bar{v}w}\\ \boldsymbol{C}_{B\upsilon\bar{w}}\end{pmatrix} \quad (5)$$

The vibrational basis functions are chosen as the eigenfunctions of the nuclear Hamiltonians

$$[T_N + U_A]|\bar{v},w\rangle = E_{A\bar{v}w}|\bar{v},w\rangle, \quad (6)$$

$$[T_N + U_B]|\upsilon,\bar{w}\rangle = E_{B\upsilon\bar{w}}|\upsilon,\bar{w}\rangle. \quad (7)$$

We will start dynamical computations adopting the most suited conformation for ET, thus we will explicitly consider in dynamics only the internal modes of the two quinones, intermolecular oscillations and modes of the proteic backbone, which according to Marcus' theory are important for bringing the two redox sites in the reactive channel, will be simulated by a low-frequency mode.[44]

Since the two quinones are far apart each other, U_A and U_B can be written as the sum of two potential-energy terms, one for each quinone, so that the vibrational wave functions are given by the product of the two vibrational eigenfunctions of the isolated moieties

$$|\bar{v},w\rangle = \chi_{\bar{v}}(\bar{q}_1)\chi_w(q_2), \quad (8)$$

$$|\upsilon,\bar{w}\rangle = \chi_{\upsilon}(q_1)\chi_{\bar{w}}(\bar{q}_2), \quad (9)$$

We will adopt harmonic approximation for U_A and U_B. That approximation is well suited to the case under study; anharmonic effects are expected to be important in cases in which dynamics takes place from a distribution of highly excited vibrational states, for instance, in the case of fast photoinduced ET, and in cases of highly exergonic processes. On the contrary, ET from Q_A^- to Q_B takes place on a time scale long enough (200 μs) for Q_A^- to relax to its equilibrium distribution of vibrational states, so that only a few low-lying excited vibrational states, those which are populated in a Boltzmann distribution at $T =$ 298 K, will play a role in dynamics. Furthermore, ET is slightly exergonic, so that even in the final state highly excited vibrational states are not expected to play a role.

Thus, the potential energy of $|A\rangle$ and $|B\rangle$ are

$$U_A = \frac{1}{2}(\bar{q}_1^{\dagger}\bar{\omega}_1{}^2\bar{q}_1 + q_2^{\dagger}\omega_2{}^2 q_2), \quad (10)$$

$$U_B = \frac{1}{2}(q_1^{\dagger}\omega_1{}^2 q_1 + \bar{q}_2^{\dagger}\bar{\omega}_2{}^2\bar{q}_2) + \Delta E_{AB} \quad (11)$$

where $\omega_{1(2)}$ is the diagonal matrix of the vibrational frequencies of $Q_{A(B)}$ and ΔE_{AB} is the energy difference between initial and final states.

In the case of RC from *Rhodobacter sphaeroides*, both Q_A and Q_B are ubiquinones, and the driving force for ET, provided only by their different environments, is only 0.07 eV.[18] Q_A and Q_B are therefore only slightly perturbed by the different environments so that it can be safely assumed that both the electronic and the vibrational wave functions of Q_A and Q_A^- are identical to those of Q_B and Q_B^- and that the vibrational states of the two quinones can be well approximated by those computed in the gas phase for the isolated mojeties.

To completely define the Hamiltonian operator, we have only to specify that the form of the coupling operator. $\mathcal{V}'_{AB}$ is usually a function of the whole set of normal coordinates of $|A\rangle$ and $|B\rangle$; however, in the case under consideration, its dependence on the nuclear coordinates can be neglected because the displacements between the normal modes of $|A\rangle$ and $|B\rangle$ are small, see infra, and therefore ET will take place in a small region of the nuclear coordinates. Thus, in the model Hamiltonian adopted here, $\mathcal{V}'_{AB}$ will simply be a multiplicative factor of the Franck−Condon integrals, whose value can be determined from the most suited nuclear configuration.

For the through-bridge tunneling (superexchange), we will explicitly consider all the three electronic diabatic states; the Hamiltonian is therefore

$$\mathcal{H} = |A\rangle[T_N + U_A]\langle A| + |B\rangle[T_N + U_B]\langle B| + |\mathrm{br}\rangle[T_N + U_{br}]\langle \mathrm{br}| + |A\rangle\mathcal{V}'_{AB}\langle B| + |A\rangle\mathcal{V}'_{Abr}\langle \mathrm{br}| + |B\rangle\mathcal{V}'_{Bbr}\langle \mathrm{br}| + c.c \quad (12)$$

where $|\mathrm{br}\rangle$ indicates the electronic state with the mobile electron localized on the iron histidine bridge.

The electronic coupling elements $\mathcal{V}'_{Abr}$ and $\mathcal{V}'_{Bbr}$ are assumed to be equal because of the symmetry of the system, and as for tunneling, their dependence over the nuclear coordinates is neglected. Since $|\mathrm{br}\rangle$ is expected to be at a significantly higher energy than $|A\rangle$ and $|B\rangle$ and it will not be populated but for a very short time, we will consider only its ground vibrational state, without allowing for nuclear relaxation upon injection of an electron on the iron−histidine bridge. With this simplification U_{br} is given by

$$U_{br} = \frac{1}{2}(q_1^{\dagger}\omega_1{}^2 q_1 + q_2^{\dagger}\omega_2{}^2 q_2) + \Delta E_{Abr} \quad (13)$$

where ΔE_{Abr} is the energy difference between $|A\rangle$ and $|\mathrm{br}\rangle$, U_A and U_B being the same as for tunneling.

Energy Parameters and Coupling Factors. As concerns relative energies, the change in Gibbs free energy for ET has been experimentally measured (0.07 eV)[18] and we will use this value for ΔE_{AB} in computations. An estimate of the relative energy of $|\mathrm{br}\rangle$ can be obtained either at SCF level of computation, from the comparison of the electron affinities (EA) of quinones and of the iron−histidine bridge, or at the multireference configuration interaction (MRCI) level of the theory. The former method is, to our opinion, more balanced because the parameter of interest is obtained as a difference of two ground state energies, but as it will be seen, to properly localize the electron on the less stable site it is necessary to neglect the interactions with the other more stable ET sites. On the contrary, MRCI computations can be performed on the whole system, but because of the size of the system, which prevents the use of large basis sets and limits the number of configurations which can be explicitly treated in a MRCI computation, the energies of the excited states are usually overestimated with respect to the ground state. Since semiempirical single-reference CI computations usually yields reasonable excitation energies,[45,46] we have used both MNDO/AM1/CI[47,48] and ab initio ROHF/CI methods to estimate relative energies and coupling elements for ET.

For the computation of realistic EAs it is necessary to explicitly consider all the charged amino acidic residues close to the redox species. For Q_A in the RC of *Rb. sphaeroides*, the nearest charged site is the iron−histidine bridge, which carries a positive charge (Fe^{2+}, GluM234$^-$). According to the X-ray structure of the RC frozen under illumination,[49] there are no other charged residues within a radius of 12 Å. Thus, the EA

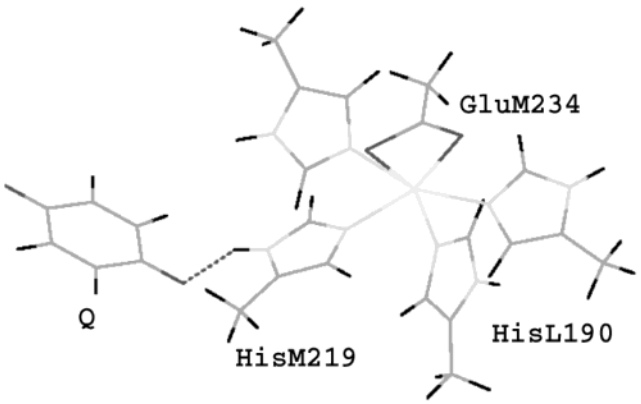

Figure 2. Schematic view of the model system adopted in the computation of the adiabatic electron affinity of *p*-benzoquinone; for the computation of the vertical electron affinity of the bridge, the H-bonded quinone has been omitted. For a better vision, the orientations of the four histidine rings have been slightly changed with respects to the optimized ones.

of the primary quinone has been computed in the field of the iron ion and of all its coordinated ligands, using *p*-benzoquinone (pBQ) as a model of the in vivo ubiquinone. The EA of ubiquinone and pBQ computed in the gas phase are very similar to each other, 2.17 and 2.15 eV, respectively, and therefore the above replacement does not affect the relative energy of the bridge with respects to those of the initial and final states.

As concerns the bridge, there are no charged amino acidic residues within a radius of 12 Å, but the GluM234, which is coordinated to the iron ion, and the GluL212, which is about 8 Å, are far from the metal ion. At this stage we have preferred to neglect the effect of GluL212 because the latter appears to increase its protonation state upon Q_B^- formation, as evidenced in the FTIR difference spectrum of Q_B^-/Q_B.[50] We have therefore considered as a model system for the bridge the metal ion with its whole coordination sphere, which includes four histidine residues, each modeled by a methyl-imidazole (MIm), and the GluM234, modeled by an acetate anion (Ac^-). In all the computations the iron ion, Fe^{2+}, has been replaced by Zn^{2+}. That replacement is legitimate, inasmuch as it has been experimentally shown that it does not significantly affect the ET rate and its efficiency,[51,52] and very useful because it greatly simplifies SCF convergence in computations. The model system adopted in computations is shown in Figure 2.

The adiabatic EA of *p*-benzoquinone in the field of the iron−histidine bridge has been computed by single-point computations, using the fully optimized geometries of $[Zn(MIm)_4Ac]^+$, pBQ, and pBQ^- moieties, see Supporting Information, and assemblying the model system according to the X-ray orientation of Q_A with the respect to the bridge. As concerns the vertical EA of the bridge, which is the physically significant parameter for superexchange, we have not included in computations the two neutral H-bonded quinones because the charge-separated state $[Zn(MIm)_4Ac]^+pBQ^-$ is the ground electronic state of the whole complex with an additional electron. The effect of the neglected H-bond interactions should slightly increase the EA of the bridge, going in the opposite direction than the electrostatic interaction with GluL212.

All the results of EA computations are summarized in Table 1.

The electronic coupling element between $|A\rangle$ and $|B\rangle$ has been evaluated as one-half of the energy difference of the two adiabatic states in the avoided crossing point. The latter has been located by fully optimizing the structure of Figure 3 under

TABLE 1: Computed Electron Affinities (eV) of PBQ and $[Zn(MIm)_4Ac]^+$

	pBQ		$[Zn(MIm)_4Ac]^+$	
	in situ[a]	isolated	in situ[a]	isolated
DFT	4.44	2.15		1.61
MNDO/AM1	4.30	2.06	1.38[b]	1.92
ab initio	3.31	1.22	−2.45[b]	−0.97

[a] From the model system of Figure 2. [b] From CI computation.

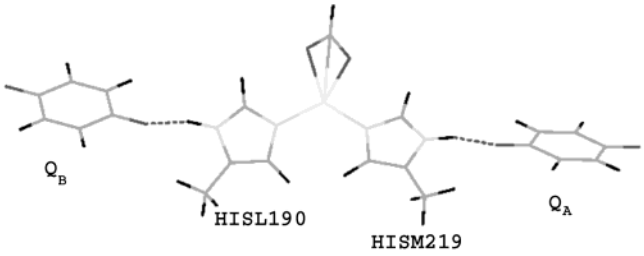

Figure 3. The model system adopted in the computation of the electronic coupling element between quinones.

TABLE 2: Electronic Coupling Elements for Tunnelling and Superexchange; Energies in eV, Dipole Moments in Debye, Coupling Factors in cm^{-1}

	tunneling	superexchange				
	$\mathcal{V}_{AB}$	μ_1	μ_2	μ_{12}	ΔE_{12}	$\mathcal{V}_{Abr}$
DFT		36.573	6.285		2.84[a]	163[b]
MNDO/AM1	3.9	40.291	7.990		2.92	157[b]
ROHF	17.7	36.996	6.09	0.215[c]	5.76	323

[a] Estimated by the EAs of pBQ and $[Zn(MIm)_4Ac]^+$ computed at DFT level. [b] Obtained from eq 14 by using μ_{12} from ROHF/CI calculation. [c] McLean and Chandler triple-valence basis set, 6-31G and 6-31G* basis sets yield 0.134 and 0.089 D, respectively.

C_2 symmetry. Both ab initio and semiempirical CI computations yield two nearly degenerate electronic states, in which the unpaired electron is delocalized on both quinones; the coupling factor is 18 and 4 cm^{-1}, from ab initio and semiempirical methods, respectively.

The electronic coupling element between $|A\rangle$ and $|br\rangle$ has been evaluated by resorting to the Mulliken−Hush model,[53−55] which, in the case of small coupling and in the two state approximation, leads to the expression[56,57]

$$|\mathcal{V}_{AB}| = \frac{\mu_{12}\Delta E_{12}}{[(\mu_1 - \mu_2)^2 + 4\mu_{12}^2]^{1/2}} \qquad (14)$$

where μ_{12} and ΔE_{12} are the transition dipole moment and the transition energy of the optical excitation involving the two adiabatic states having maximum overlap with $|A\rangle$ and $|B\rangle$, $|1\rangle$ and $|2\rangle$, and μ_1 and μ_2 are the dipole moments of $|1\rangle$ and $|2\rangle$, respectively.

The results of computations are summarized in Table 2; $\mathcal{V}_{Abr}$ is estimated to be of the order of a few hundreds of cm^{-1}, the higher value yielded by ab initio computations is mainly a consequence of the high overestimate of the $|1\rangle \rightarrow |2\rangle$ transition energy by ab initio CI computations.

Choice of the Active Modes for ET. The vibrational modes that are important for ET can be identified by carrying out a Franck−Condon analysis. In fact, modes that are neither displaced nor mixed upon ET are not expected to play a role in dynamics, because the overlap, i.e., the "horizontal" Franck−Condon integral, between vibrational states of $|A\rangle$ and $|B\rangle$, which differ for one or more quanta on these modes, will be negligibly small.

TABLE 3: Frequencies (cm^{-1}), Displacements ($Å \cdot amu^{1/2}$), and Mixing Coefficients of the Normal Modes of pBQ and pBQ^-

	ω				
mode	pBQ	pBQ^-	$\Delta\omega$	**K**	**J**
$1b_{3u}$	93.545	129.255	35.710	0.001	
$1b_{2g}$	222.364	308.631	86.267	0.000	
$1a_u$	336.187	395.068	58.881	0.000	
$1b_{2u}$	411.499	389.082	−22.417	0.000	
$1a_g$	454.220	468.121	13.901	−0.473	
$1b_{3g}$	455.618	470.774	15.156	0.000	0.98 $1b_{3g}$ −0.16 $2b_{3g}$
$2b_{3u}$	513.679	513.847	0.168	0.002	
$2b_{3g}$	601.156	630.286	29.130	0.000	0.17 $1b_{3g}$ +0.98 $2b_{3g}$
$1b_{1u}$	754.538	764.365	9.827	−0.010	
$1b_{1g}$	755.060	789.560	34.500	−0.001	
$2a_g$	774.099	821.519	47.420	0.150	
$2b_{1g}$	781.091	736.583	−44.508	0.000	0.97 $2b_{1g}$ +0.20 $3b_{1g}$
$3b_{3u}$	901.426	850.859	−50.566	−0.001	
$2b_{1u}$	947.869	962.813	14.943	0.000	
$2a_u$	1009.591	944.865	−64.726	0.000	
$3b_{1g}$	1010.118	936.341	−73.776	0.000	−0.18 $2b_{1g}$ +0.98 $3b_{1g}$
$2b_{2u}$	1085.794	1077.671	−8.123	0.000	
$3a_g$	1168.916	1155.331	13.586	−0.094	
$3b_{3g}$	1237.067	1264.164	27.097	0.000	0.96 $3b_{3g}$ +0.26 $4b_{3g}$
$3b_{2u}$	1320.373	1231.884	−88.489	0.000	0.95 $1b_{2u}$ −0.28 $4b_{2u}$
$3b_{1u}$	1385.696	1370.247	−15.448	0.000	0.95 $3b_{1u}$ −0.30 $4b_{1u}$
$4b_{3g}$	1397.902	1454.347	−56.446	0.000	−0.25 $3b_{3g}$ +0.96 $4b_{3g}$
$4a_g$	1648.909	1501.946	−146.963	0.000	0.85 $4a_g$ −0.51 $5a_g$
$4b_{2u}$	1680.332	1491.066	−189.266	0.004	0.28 $1b_{2u}$ +0.96 $4b_{2u}$
$4b_{1u}$	1736.041	1538.940	−197.100	0.005	0.30 $3b_{1u}$ +0.95 $4b_{1u}$
$5a_g$	1738.235	1651.182	−87.052	−0.162	0.51 $4a_g$ +0.85 $5a_g$
$5b_{1u}$	3196.719	3145.006	−51.713	0.000	
$5b_{3g}$	3197.320	3144.347	−52.972	0.000	
$5b_{2u}$	3213.312	3165.081	−48.231	0.000	
$6a_g$	3215.552	3169.881	−45.671	0.009	

The normal modes of two different electronic state of a molecule, $|1\rangle$ and $|2\rangle$, are related by Duschinsky's affine transformation[58]

$$q_1 = \mathbf{J}q_2 + \mathbf{K} \tag{15}$$

More details about the calculation of **J** and **K** can be found in ref 59.

The rotation matrix **J** and the displacement vector **K** are reported in Table 3, together with the harmonic frequencies computed at the DFT level.

There are 4 modes significantly displaced, shown in Figure 4, of course all belonging to the A_g irreducible representation of D_{2h} point group. Among them only one is significantly displaced (0.45 $Å/amu^{1/2}$), falling at 454 cm^{-1}. That mode is expected to play the major role in ET dynamics, both because FC integrals between vibrational states differing for one or more quanta on this mode will be larger and because the energy difference between vibrational states differing for one quantum on this mode is comparable to the energy gap between reactants and products. As concerns the Duschinsky effect, there are 12 modes that are only slightly mixed with each other, cf. Table 3. Only two modes fall in the region of lower frequencies, 455 and 630 cm^{-1}, so that they are expected to play the most important role, among all other mixed modes, in ET dynamics.

Direct Tunneling. As seen in the previous section, there are several modes that change their equilibrium positions or mix each other upon ET; since it is not possible to include vibrational excited states for each of them in the dynamics, we have started by performing preliminary computations aimed to understand the role of each single displaced mode and each pair (there are no cases in which more than two modes are mixed, cf. Table 3) of mixed modes. The results are summarized in Table 4. In these computations, we allow only one mode at a time to be excited, but all 60 modes of the two quinones are considered in building up the Hamiltonian matrix.

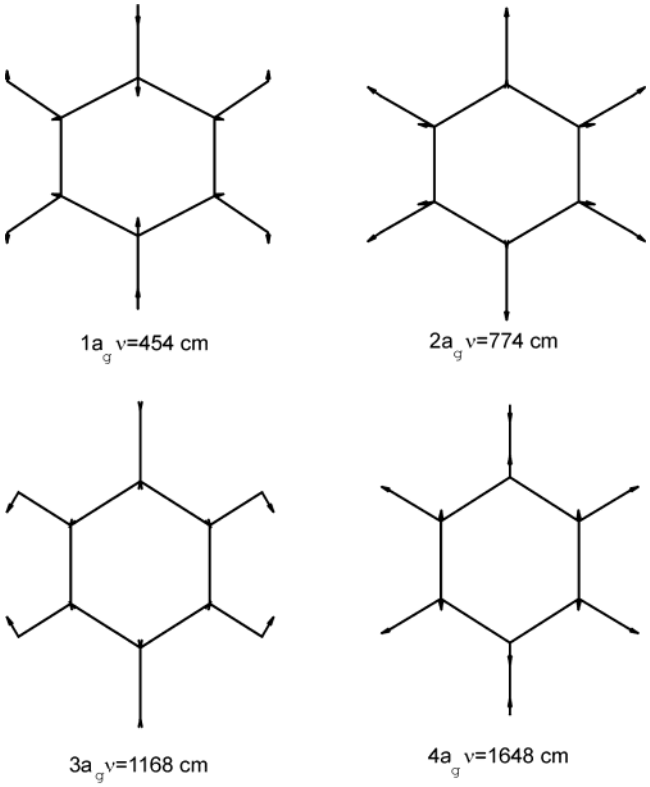

Figure 4. The normal modes of *p*-benzoquinone mostly displaced with respects to those of *p*-benzosemiquinone.

The tunneling probabilities reported in Table 4 have been computed assuming that at $t = 0$ the system is completely localized in the diabatic state $|A\rangle$, in the Boltzmann distribution at $T = 298$ K, and by summing over all the vibrational states of $|B\rangle$.[60] Three values of the coupling element have been considered: 17.7, as obtained by ab initio MRCI computation, 100, and 550 cm^{-1}. Higher values of the electronic coupling element have been considered because the computed ones yield very low transition probabilities, less than 1%, so that an estimate of the order of magnitude of $\mathcal{V}_{AB}$ at which ET probabilities become significant is in order for subsequent discussion.

Even with $\mathcal{V}_{AB} = 550$ cm^{-1}, which is about 2 orders of magnitude larger than what expected both from computations and from the exponential decay of the electronic coupling element with the intermolecular distance (1.7 cm^{-1} from Hopfield's expression,[61] see infra), the transition probabilities are low, but for the case in which the most displaced $1a_g$ mode ($\omega = 454$ cm^{-1}) is active. In that case the maximum probability is ca. 0.6, for $\mathcal{V}_{AB} = 550$ cm^{-1}, in 120 fs.

In Figure 5 the transition probabilities obtained by considering as active all the displaced modes are compared with those obtained by exciting only the lowest-frequency one. The computed probabilities differ by roughly 10%, so that on the basis of this result we have discarded all the high-frequency modes and considered the role of the low-frequency ones. Those modes could play a part in ET dynamics because small differences in their frequencies can lead close to resonant conditions, in an energy interval above the vibronic ground state of $|A\rangle$ significant in a Boltzmann average.

In Figure 6, Boltzmann-averaged transition probabilities obtained by considering the two frequency modes, $1b_{3u}$ and $1b_{2g}$

TABLE 4: Tunneling Probabilities for Different Excited Modes

	max Probability			time (fs)		
excited modes	$\mathcal{V}_{AB} = 17$	$\mathcal{V}_{AB} = 100$	$\mathcal{V}_{AB} = 550$	$\mathcal{V}_{AB} = 17$	$\mathcal{V}_{AB} = 100$	$\mathcal{V}_{AB} = 550$
$1a_g$	0.0019	0.058	0.63	145	148	119
$2a_g$	7×10^{-5}	0.0023	0.068	85	83	83
$3a_g$	2.5×10^{-5}	0.00078	0.023	28	29	29
$4a_g$	2.5×10^{-5}	0.0006	0.018	38	33	30
$5a_g$	2.0×10^{-5}	0.0006	0.018	21	31	29
$1b_{3g}$,$2b_{3g}$	2.0×10^{-5}	0.0006	0.018	88	29	30
$1a_g$,$1b_{3u}$,$1b_{2g}$	0.027	0.13	0.5	5×10^3	750	35
no excited modes	$2.0 \cdot 10^{-5}$	0.0006	0.018	21	31	29

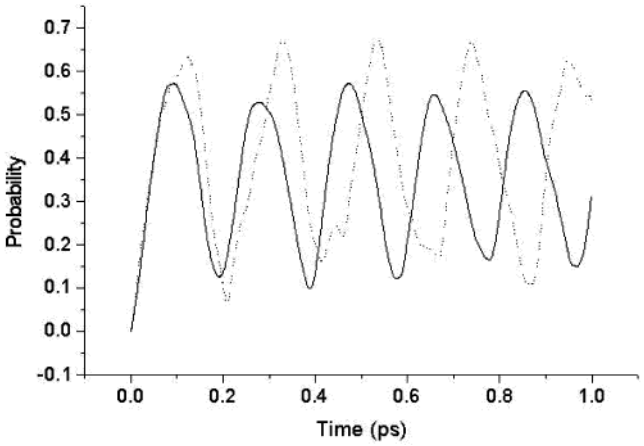

Figure 5. Transition probabilities of electron transfer from Q_A^- to Q_B for $\mathcal{V}_{AB} = 550$ cm^{-1}. Full line: only the lowest-frequency $1a_g$ mode has been excited; dotted line: all the a_g displaced modes have been excited.

and $1a_g$ as active modes are reported for different values of the coupling element. The effect of the low-frequency mode is remarkable; for $\mathcal{V}_{AB} = 17.7$ cm^{-1}, the maximum probability increases from 0.2 to ca. 3%, about 1 order of magnitude, but the transition is strongly slowed, occurring in about 5 ps. For a higher value of the coupling element, transition probabilities increase and the behavior of the dynamics comes out to be very different from the previous one; periodic oscillations no longer occur, at least in the picosecond time scale, and the population of the final state slightly oscillates around the value corresponding to the maximum transition probability, cf. parts b and c of Figure 6.

Because of the large effect obtained by including in dynamics the lowest excited mode, we have performed a few exploratory dynamics using ubiquinone instead of pBQ. In fact, the FC analysis for ubiquinones show several slightly displaced (ca. 0.1 Å/amu$^{1/2}$) low-frequency modes, essentially related to torsional vibrations of the methyl groups; all other modes are almost unchanged. Preliminary computations have not shown any significant variation; the transition probabilities are always lower than those obtained by using the rigid pBQ model.

By judging from the maximum transition probabilities reported in Table 4, mixed modes (Duschinsky's effect) appear to play a very marginal role in ET dynamics; the highest transition probability for $\mathcal{V}_{AB} = 550$ cm^{-1} is only 2% after 30 fs, which is comparable to the dynamics with no excited modes.

Thus, among all 60 modes of the two quinones, only a few of them are important in promoting ET via direct tunneling, the most displaced one, the $1a_g$ mode at 454 cm^{-1}, which can be considered as the active one for ET, and the lowest frequency modes, ($1b_{3u}$, $1b_{2g}$) which plays the role of filling up the gap between vibronic states of $|A\rangle$ and $|B\rangle$, slightly increasing ET probabilities.

TABLE 5: Superexchange Probabilities for Different Excited Modes (Time in fs)

excited modes	ΔE_{Abr}	$\mathcal{V}_{Abr}$	P_{max}	τ
$1a_g$	2.5	160	$1.6 \cdot 10^{-5}$	150
$1a_g$	2.5	1000	0.016	150
$1a_g$	2.5	2000	0.21	130
$1a_g$	2.0	160	2×10^{-5}	130
$1a_g$	2.0	1000	0.025	150
$1a_g$	2.0	2000	0.30	120
$1a_g$	1.0	160	7×10^{-5}	130
$1a_g$	1.0	1000	0.10	150
$1a_g$	1.0	2000	0.61	110
$1a_g$	0.5	160	3×10^{-4}	130
$1a_g$	0.2	160	4.5×10^{-2}	200
$1b_{3g}$ $2b_{3g}$	2.5	160	1.6×10^{-8}	30
$1b_{3g}$, $2b_{3g}$	2.5	1000	0.00016	30
$1b_{3g}$, $2b_{3g}$	2.5	2000	0.0025	30
$1b_{3u}$, $1a_g$	2.5	160	3×10^{-6}	2000
$1b_{3u}$, $1a_g$	2.5	1000	0.03	2000
$1b_{3u}$, $1a_g$	2.5	2000	0.2	100
no excited modes	2.5	160	1×10^{-7}	29

Superexchange. The results of several dynamics carried out with the computed relative energies and coupling elements of Table 2 are summarized in Table 5. As for tunneling, the probabilities of Table 5 have been determined assuming that at $t = 0$ the system is completely localized in the vibronic states of $|A\rangle$, with relative populations given by the Boltzmann distribution at $T = 298$ K, and by summing over all the vibrational states of $|B\rangle$. The maximum probabilities of Table 5 clearly show that, with the computed energy differences and relative coupling elements, superexchange is not a possible route for ET from Q_A to Q_B. To obtain significant transition probabilities, the coupling element $\mathcal{V}_{Abr}$ must be increased by more than 1 order of magnitude and ΔE_{Abr} decreased to one-third of the computed value. The results also show that mixed modes as well as low-frequency ones play a marginal role in ET dynamics.

When the direct and the through-bridge channels are opened together, an interesting quantum effect occurs, due to the interference between probability amplitudes of the direct and the indirect processes. In particular, if the two coupling elements have opposite signs, the amplitude probability increases, whereas it decreases if the two couplings have the same sign. That effect was already reported in the literature.[62,63] Recent examples show that such a situation can occur for large flexible molecules[64] or for the case where there is an additional functional group in the bridge compound.[65] Interference between competing pathways can have important effects on ET probabilities,[66] we have not further investigated these aspects of ET dynamics because, in the case we have examined, the direct channel predominates.

In the Supporting Information, the results of several dynamics, obtained by exciting different modes and covering a broad range of the coupling element, are collected, both for tunneling and superexchange.

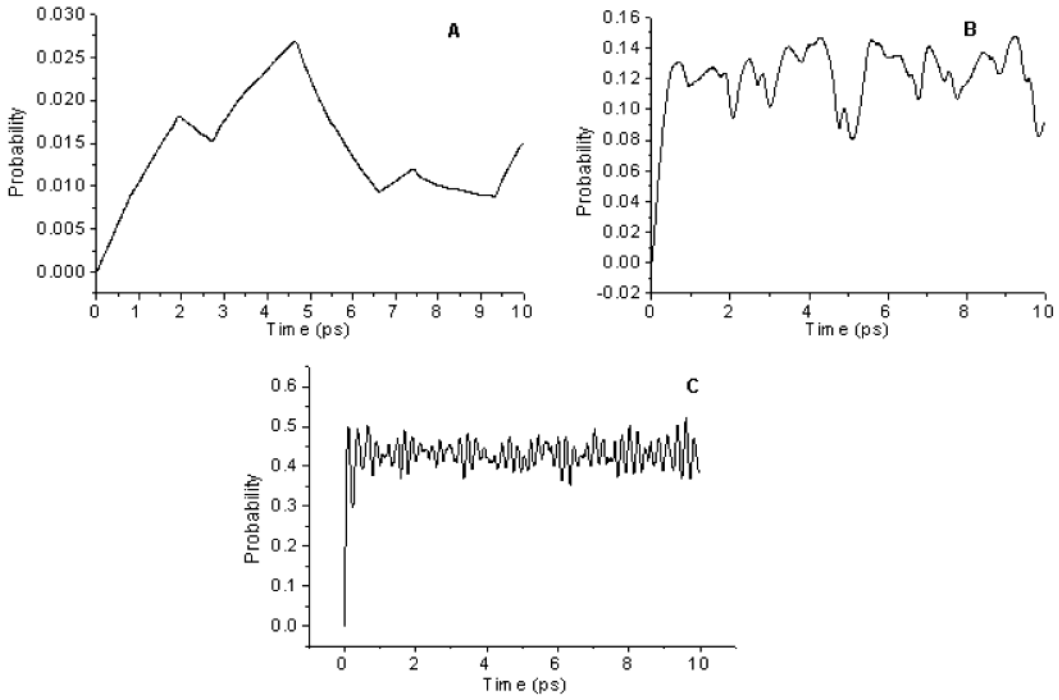

Figure 6. Transition probabilities of electron transfer from Q_A to Q_B; the two lowest-frequency $1b_{3u}$ and $1b_{2g}$ modes and the $1a_g$ mode have been excited. (A) $\mathcal{V}_{AB} = 17$ cm^{-1}; (B) $\mathcal{V}_{AB} = 100$ cm^{-1}; and (C) $\mathcal{V}_{AB} = 550$ cm^{-1}.

Role of Nonquinone Modes. The above results lead to the conclusion that the internal modes of the two quinones are not effective to promote ET. Both tunneling and superexchange exhibit very low probabilities, whereas it is known that ET occurs with high efficiency, close to unity.[2] High probabilities are obtained only by increasing the computed coupling element by at least 1 order of magnitude, but these values are in contrast not only with the computed ones but also with those obtained by empirical expressions relating $\mathcal{V}_{AB}$ with the edge-to-edge contact between two redox aromatic sites. Hopfield's expression (in eV)

$$\mathcal{V} = \frac{2.7}{(N_a N_b)^{1/2}} \exp(-0.72R) \qquad (16)$$

where R (Å) is the edge-to-edge distance between two large aromatic groups a and b of N_a and N_b atoms, yields $\mathcal{V}_{AB} = 1.7$ cm^{-1} by keeping $R = 13.1$ Å, the shortest (O−O) distance, and neglecting the normalization factor ($^1/_8$) (ab initio computations suggest that the unpaired electron is mainly localized on the two quinone oxygens, so that a factor $^1/_2$ seems to be more appropriate than $^1/_8$). That value is in very good agreement with MNDO/AM1/CI computations (3.9 cm^{-1}) and 1 order of magnitude smaller than the ab initio ROHF/CI estimate. The same expression yields $\mathcal{V}_{Abr} = 185$ cm^{-1} by considering the shortest distance between the π atoms of the quinone and of the H-bonded histidine (2.8 Å) and by using the appropriate normalization factor, again in agreement with both DFT and MNDO/AM1 estimates, 163 and 157 cm^{-1}, respectively. Thus, if the computed coupling elements are reasonable, as the above analysis would suggest, and since anharmonic effects cannot be as large as necessary to increase the effective coupling by at least 1 order of magnitude, the FC integrals important for ET being well above 0.1, the low transition probabilities obtained in ET dynamics, must be attributed to the fact that the Franck−Condon weighted density of states provided by the normal modes of the two quinones is too small for ET to occur. Then the question about the possible role of "external" modes, the vibrational modes of the protein backbone and/or of the water molecules, which are mostly around the Q_B site, must be addressed.

External modes should play a role similar to that of the lowest-frequency modes of pBQ and pBQ$^-$, namely, that of filling up the energy gap between vibronic states of the donor and the acceptor groups, increasing transition probabilities. Of course, since there are no chances to compute either a Franck−Condon factor or a vibrational frequency for such modes, we will therefore estimate their effects by simply considering how the transition probability for ET via tunneling and superexchange will change as the energy difference between the initial and final state decreases up to $\Delta E_{AB} = 0$. That procedure will only yield an upper limit to transition probabilities, which can be significantly lowered upon including the appropriate FC factors.

The transition probabilities as a function of time, for small ΔE_{AB} values, are reported in Figures 7 and 8 for tunneling and superexchange, respectively. In both these dynamics, we used the computed values of the coupling elements, i.e., $\mathcal{V}_{AB} = 17.7$ cm^{-1} for tunneling and $\mathcal{V}_{Abr} = 160$ cm^{-1} $\Delta E_{Abr} = 2.5$ eV for superexchange. When perfect degeneracy between vibronic states of $|A\rangle$ and $|B\rangle$ is imposed in dynamics, $\Delta E_{AB} = 0$, the transition probabilities rise close to unity, both for tunneling and superexchange, but the transition times become much longer, 6 ps for tunneling and 100 ps for superexchange, cf. Figures 7a and 8a. The transition probabilities for ET rapidly fall off as degeneracy is slightly removed. In the case of tunneling, the maximum probability is 0.3 for $\Delta E_{AB} = 5 \times 10^{-4}$ eV, cf. Figure 7b, and goes down to 6×10^{-3} for $\Delta E_{AB} = 5 \times 10^{-3}$ eV, Figure 7c. The rapid decrease of ET probabilities is much more pronounced in the case of superexchange, the maximum probability for ET is only 0.17 for $\Delta E_{AB} = 5 \times 10^{-5}$ eV, about 0.4 cm^{-1}, Figure 8b, and goes down to 2×10^{-3} for $\Delta E_{AB} = 5 \times 10^{-4}$ eV, Figure 8c.

Conclusions

The results discussed so far clearly show that ET from Q_A to Q_B via tunneling or superexchange mechanisms can only occur

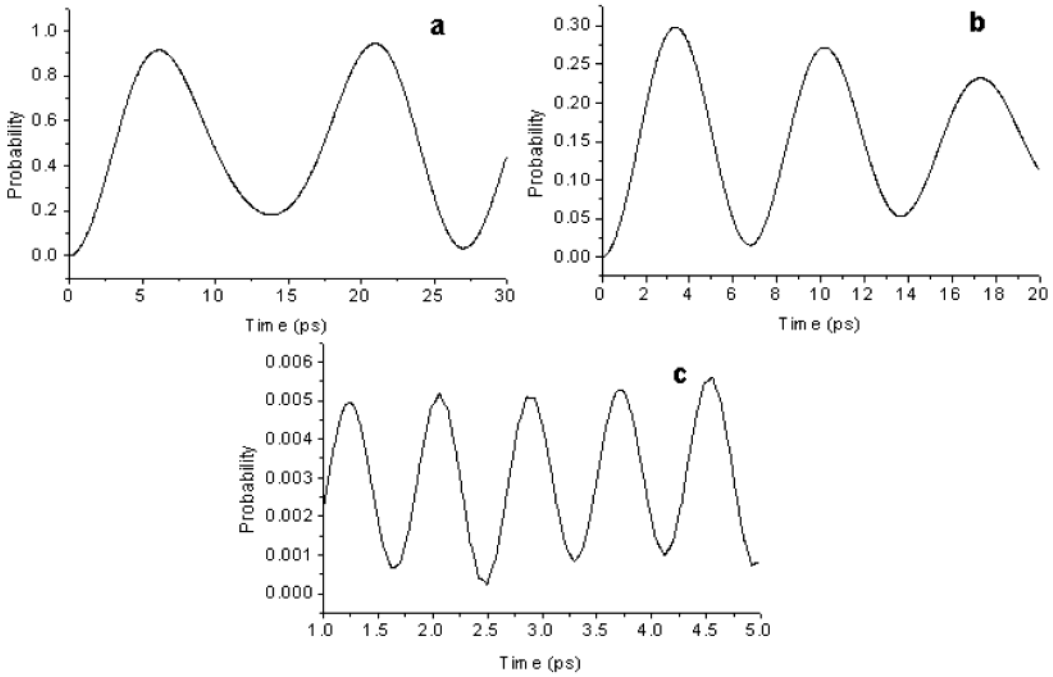

Figure 7. Transition probabilities of ET via tunneling for different values of ΔE_{AB}: (a) $\Delta E_{AB} = 0.0$; (b) $\Delta E_{AB} = 5 \times 10^{-4}$ eV; (c) $\Delta E_{AB} = 5 \times 10^{-3}$ eV. The lowest-frequency mode $1b_{3u}$ and the most displaced mode $1a_g$ have been excited in all the dynamics, $\gamma_{AB} = 17$ cm^{-1}.

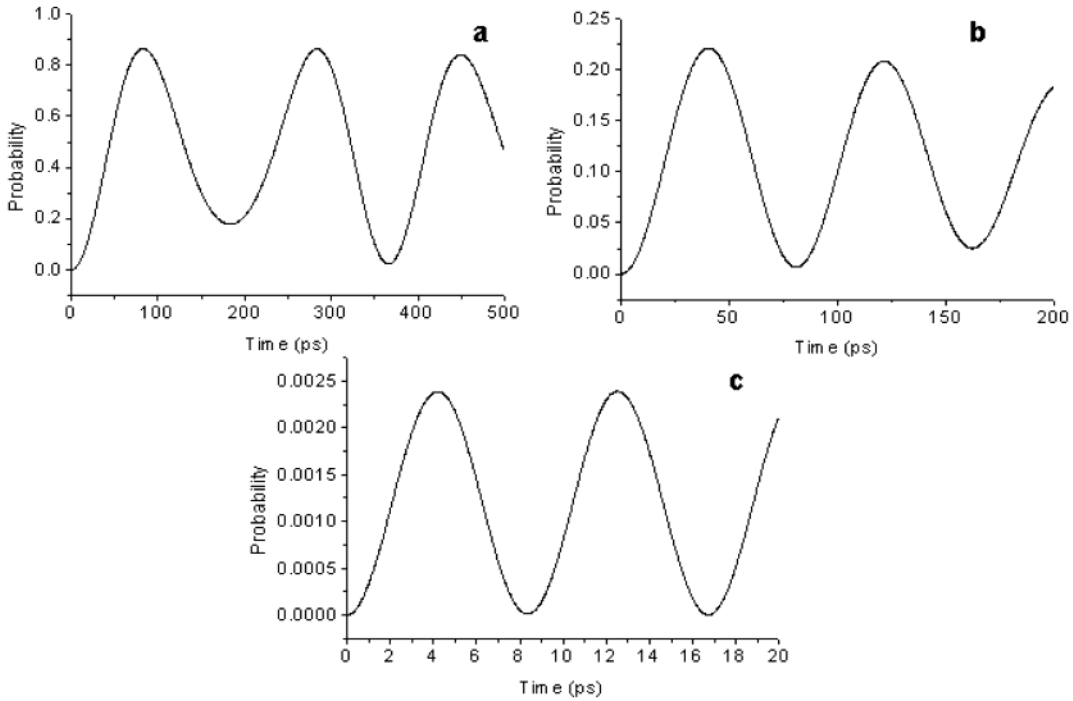

Figure 8. Transition probabilities of ET via superexchange for different values of ΔE_{AB}: (a) $\Delta E_{AB} = 0.0$; (b) $\Delta E_{AB} = 5 \times 10^{-5}$ eV; (c) $\Delta E_{AB} = 5 \times 10^{-4}$ eV. The lowest-frequency mode $1b_{3u}$ and the most displaced mode $1a_g$ have been excited in all the dynamics, $\gamma_{AB} = 17$ cm^{-1}.

when the vibronic states of $|A\rangle$ and $|B\rangle$ are tightly degenerate. That requirement is much more stringent for superexchange, in that case an energy difference of 0.4 cm^{-1} makes the ET probability to fall off below 20%. For tunneling, the range of degeneracy relaxes to a few cm^{-1} and, since the latter energy interval is more reasonable, tunneling is to be preferred to superexchange, also because the computed transition times via tunneling are much shorter than those via superexchange, 6 ps vs 100 ps, respectively.

Thus the first conclusion that can be drawn is that direct tunneling is more effective than superexchange. However, even the direct tunneling pathway poses questions: first of all, is such a stringent energy condition met in photosynthetic RCs? The case of ET between quinones in RCs is in fact quite different from other photoinduced ET processes. In RCs, ET from Q_A^- to Q_B takes place from the lowest vibrational states of $|A\rangle$ because photoinduced ET from the special pair to Q_A via bacteriopheophytin occurs in a time scale much faster than ET from Q_A^- to Q_B so that the former has time enough to relax into a thermal distribution of vibrational states. Therefore only a few excited vibrational states above the ground vibrational state will be populated and, since ET from Q_A^- to Q_B is only slightly exothermic, that holds even for the final electronic state. In such a small energy interval, a very high Franck−Condon

weighted density of states is not expected, even if the low-frequency modes of the protein backbone are considered. Those modes will damp down time oscillations of ET probabilities, making ET irreversible, cf. Figure 6, rather than directly promote it. Moreover, if ET were really controlled by stringent resonance conditions, one would expect that the efficiency of ET crucially depends on quinone substitution and that is in contrast with experimental results.[67] On the basis of the above argumentations, a sort of mechanism, a driven chemical modification, which accounts for the high efficiency of ET in RCs, would be, to our opinion, better suited to the case in question. The hypothesis of a conformational gating of ET rate associated to the large Q_B displacement from the distal to the proximal site, as proposed by Graige et al.,[28] is certainly valid (our analysis starts in fact considering the two quinones H-bonded to two opposite histidines of the metal bridge, as also suggested by other theoretical analysis),[66] but according to the above results, it is not sufficient to yield high ET probabilities.

An alternative to direct tunneling mechanism could be the previously mentioned PAET mechanism. Both chemical intuition and computations suggest that the PAET mechanism is plausible. Hydrogen atom transfers are in fact common steps in the chemistry of radicals, occurring with an energy barrier of a few kcal/mol.[68,69] Computations predict that all the steps involved in the PAET mechanism are slightly exergonic[38,39] and that the proton-transfer step from the iron−histidine to Q_A is extremely fast, much faster than direct ET tunneling.[39]

There are a few, not conclusive, pieces of evidence that the arrival of an additional electron on Q_A strongly perturbs the network of H bonds around Q_A^-. First of all, the already mentioned broad positive band observed in the Q_A^-/Q_A FTIR difference spectrum[37] is very similar to that observed in the IR spectrum of imidazole in the polycristalline state[71,72] so that the involvement of the N−H stretching of the histidine H-bonded to Q_A can be envisioned. Moreover, the analysis of ENDOR spectra point toward the assignment of an important role to the strong H bond formed by Q_A^- with HisM219 in the electron-transfer process.[42] Of course, deeper experimental investigations are needed for a better assessment of the role that the PAET mechanism could play in the ET process between quinones in RCs. Electronic absorption spectra do not show evidence in favor of the formation of a neutral semiquinone, but to our knowledge, only steady-state spectra have been reported in the literature,[70] while the detection of a short-living intermediate, such as the neutral semiquinone in the PAET mechanism, requires ad hoc time-resolved techniques for a conclusive assessment. It must also be remarked that the schematization of PAET in a sequence of proton and whole hydrogen atom transfers might be too drastic. It is very possible that ET and PT steps occur in a rapid succession so that the whole ET process takes place in a few vibrations of the H-bonded heavy atoms, without forming any metastable transient species such as Q_AH and Q_BH. Even in that case, PAET would be very different from tunneling or superexchange, inasmuch the real electron carriers are the H-bonded protons, so that ET should not occur if the H-bond chain connecting quinones is broken.

Computational Details

Ab initio Hartree−Fock and CI calculations have been carried out by the Gamess package;[73] the Gaussian94[74] and the MOPAC[75] packages have been used for calculations based on DFT[76,77] and MNDO approximation[47] with AM1 parametrization,[78] respectively. The B3LYP hybrid exchange-correlation potential[79] has been employed in all DFT computations. All geometry optimization runs started from the X-ray coordinates of the RC from *Rhodobacter sphaeroides* crystallized under illumination.[49]

In all the ab initio computations, the geometries of the stationary points of the potential energy hypersurface have been located by full optimization, using the LanL2DZ core potential basis set[80−82] for Zn and the standard 3-21G basis set for all the other atoms. Energies have been calculated by single-point computations with no core potential and the 6-31G basis set for all the atoms but for Zn, for which the McLean−Chandler triple-valence basis set[83] has been employed.

For the computation of the electronic coupling element for direct tunneling, we have first fully optimized the structure of Figure 3 at the ROHF/3-21G level of the theory imposing C_2 symmetry and then performed MRCI computations using the 6-31G/MC basis set. The active space employed in CI includes 11 molecular orbitals, of which four doubly and one singly occupied, whereas the external space consisted of the lowest 10 virtual orbitals not included in the active space. Only single and double excitations have been considered for building up the reference space, whereas only singly excited determinants obtained by promoting electrons from the reference to the external space have been included in CI computations.

All the geometry optimizations performed by using the DFT/B3LYP method have been carried out employing the standard 6-31G basis set, whereas energies have been evaluated using the 6-31+G(d) basis set. According to several test computations, that method yields reliable electron affinities at a reasonable computational cost.[84] It must be remarked that the electron affinity reported here could still be affected by the field of the protein, even though the effects of the nearest charged groups has been taken into account. These effects could in principle be addressed by QM/MM computations, but in our opinion, ad hoc parameters are necessary to properly allow for screening effects. Work is in progress along that direction.

Electronic coupling elements for superexchange have been estimated by using expression 14. The necessary parameters have been valued by different methods as follows: (i) the transition dipole moment has been estimated only at the ROHF/MRCI level of the theory, using the McLean−Chandler basis set for all atoms and used also in conjunction with parameters obtained by DFT and MNDO/AM1 calculations; (ii) dipole moments of the excited adiabatic state have been estimated by CI computations at ab initio and MNDO levels of the theory, whereas the DFT value refers to that computed at SCF level for the $[Zn(MIm)_4Ac]$ neutral complex; (iii) ab initio and MNDO transition energies have been estimated by CI computations, whereas the DFT value has been inferred from the difference between the electron affinity of the parabenzoquinone, computed in the presence of the $[Zn(MIm)_4Ac]^+$ bridge, and the vertical electron affinity of the isolated bridge.

The normal modes of vibration of pBQ and pBQ^- have been computed at the DFT/B3LYP level of computations, using the standard 6-31++G** basis set.

ET dynamics have been carried out by numerical solution of the time-dependent Schrödinger equation, employing the Lanczos method.[85] Vibrational states have been obtained by expanding the wave function over a set of either Gaussian functions[86,87] or two sets of harmonic oscillator wave functions centered in the two minimum-energy configurations of $|A\rangle$ and $|B\rangle$.[88] The two methods yield very similar results; the former is more easy to be implemented, whereas the latter requires lower computational costs but, in the actual implementation, is limited by the number of Franck−Condon integrals which can be stored

in memory. Franck−Condon factors have been computed by the FCDYN package[89] based on hermite recurrence relations.[88]

Acknowledgment. The financial support of MIUR, PRIN 2000, and of University of Salerno is gratefully acknowledged.

Supporting Information Available: Optimized coordinates of $[Zn(Im)_4Ac]^+$, pBQ, and pBQ^- and the results of several dynamic tests for both tunneling and superexchange (jpg files) are available free of charge via Internet at http://pubs.acs.org.

References and Notes

(1) Voet, D.; Voet, J. *Biochemisty;* John Wiley and Sons: INC: 1995.
(2) Feher, G. A. J. P.; Okamura, M. Y.; Rees, D. C. *Nature* **1989**, *339*, 111.
(3) Paddock, M. L.; Rongey, S. H.; Feher, G.; Okamura, M. Y. *Proc. Natl. Acad. Sci. U. S. A.* **1989**, *86*, 6602.
(4) Mitchell, P. *Nature* **1961**, *191*, 144.
(5) Deisenhofer, J.; Michel, H. *EMBO J.* **1989**, *8*, 2149.
(6) Deisenhofer, J.; Epp, O.; Sinning, I.; Michel, H. *J. Mol Biol.* **1995**, *246*, 429.
(7) Feher, G.; Allen, J. P.; Yeats, T. O.; Chirino, A.; Rees, D. C.; Komiya, H. *Proc. Natl. Acad. Sci. U. S. A.* **1988**, *85*, 7993.
(8) Feher, G.; Allen, J. P.; Yeats, T. O.; Chirino, A.; Rees, D. C.; Komiya, H. *Proc. Natl. Acad. Sci. U. S. A.* **1988**, *85*, 8487.
(9) Stowell, M. H. B.; McPhillips, T.; Rees, D. C.; Soltis, S. M.; Abresch, E.; Feher, G. *Science* **1997**, *276*, 812.
(10) McElroy, J. D.; Feher, G.; Mauzerall, D. C. *Biochim. Biophys. Acta* **1969**, *172*, 180.
(11) Norris, J. R.; Uphaus, R. A.; Crespi, H. L.; Katz, J. J. *Proc. Natl. Acad. Sci. U. S. A.* **1971**, *68*, 625.
(12) Feher, G.; Hoff, A. J.; Isaacson, R. A.; Ackerson, L. C. *Ann. N. Y. Acad. Sci.* **1975**, *244*, 239.
(13) Norris, J. R.; Scheer, H.; Katz, J. J. *Ann. N. Y. Acad. Sci.* **1975**, *244*, 260.
(14) Holzapfel, W.; Finkele, U.; Kaiser, W.; Oesterhelt, D.; Scheer, H.; Stilz, H. U.; Zinth, W. *Proc. Natl. Acad. Sci. U. S. A.* **1990**, *87*, 5168.
(15) Holten, D.; Hoganson, C.; Windsor, M. W.; Schenck, C. C.; Parson, W. W.; Migus, A.; Fork, R. L.; Shank, C. V. *Biochim. Biophys. Acta* **1980**, *592*, 461.
(16) Shuvalov, V. A.; Parson, W. W. *Proc. Natl. Acad. Sci. U. S. A.* **1981**, *78*, 957.
(17) Woodbury, W. T.; Parson, W. W. *Biochim. Biophys. Acta* **1984**, *767*, 345.
(18) Kleinfeld, D.; Okamura, M. Y.; Feher, G. *Biochim. Biophys. Acta* **1984**, *766*, 126.
(19) Kleinfeld, D.; Okamura, M. Y.; Feher, G. *Biochemistry* **1984**, *23*, 5780.
(20) Rockley, M. G.; Windsor, M. W.; Codgell, R. J.; Parson, W. W. *Proc. Natl. Acad. Sci. U. S. A.* **1975**, *72*, 2251.
(21) Kaufmann, K. J.; Dutton, P. L.; Netzel, T. L.; Leigh, J. S.; Rentzepis, P. M. *Science* **1975**, *188*, 1301.
(22) Holten, D.; Windsor, M. W.; Parson, W. W.; Thornber, J. P. *Biochim. Biophys. Acta* **1978**, *501*, 112.
(23) Kirmaier, C.; Holten, D. *Photosynth. Res.* **1987**, *13*, 225.
(24) Okamura, M. Y.; Feher, G. *Annu. Rev. Biochem.* **1992**, *61*, 861.
(25) Gust, D.; Moore, T. A.; Moore, A. L. *Acc. Chem. Res.* **1993**, *26*, 1988.
(26) Gratzel, M. *Acc. Chem. Res.* **1981**, *14*, 376.
(27) Ballardini, R.; Balzani, V.; Credi, A.; Gandolfi, M. T.; Venturi, M. *Acc. Chem. Res.* **2001**, *34*, 445.
(28) Graige, M. S.; Feher, G.; Okamura, M. Y. *Proc. Natl. Acad. Sci. U. S. A.* **1998**, *95*, 11679.
(29) Franzen, S.; Boxer, S. G. *J. Phys. Chem.* **1993**, *97*, 6304.
(30) McPherson, P. H.; Nagarajan, V.; Parson, W. W.; Okamura, M. Y.; Feher, G. *Biochim. Biophys. Acta* **1990**, *1019*, 91.
(31) Peluso, A.; Carotenuto, M.; Brahimi, M.; Del Re, G. *J. Phys. Chem.* **1998**, *102*, 10333.
(32) Del Re, G.; Brahimi, M.; Peluso, A. *Chem. Phys. Lett.* **1999**, *299*, 511.
(33) Soudackov, A.; Hammes-Shiffer, S. *J. Am. Chem. Soc.* **1999**, *121*, 10598.
(34) Kotelnikov, A. I.; Medvedev, E. S.; Medvedev, D. M.; Stuchebrukhov, A. A. *J. Phys. Chem. B* **2001**, *105*, 5789.
(35) Breton, J.; Boullais, C.; Mioskowski, C.; Sebban, P. Baciou, L.; Nabedryk, E. *Biochemistry* **2002**, *41*, 12921.
(36) Nabedryk, E.; Breton, J.; Sebban, P.; Baciou, L. *Biochemistry* **2003**, *42*, 5819.
(37) Breton, J.; Nabedryk, E. *Photosynth. Res.* **1998**, *55*, 301.
(38) Peluso, A.; Di Donato, M.; Saracino, G. A. A. *J. Chem. Phys* **2000**, *113*, 3212.
(39) Correa, A.; Di Donato, M.; Peluso, A. *Chem. Phys. Lett.* **2003**, *369*, 549.
(40) Peluso, A.; Di Donato, M.; Saracino, G. A. A.; Improta, R. *J. Theor. Biol.* **2000**, *207*, 101.
(41) Hung, S.; McPherson, A. N.; Lin, S.; Liddell, P. A.; Seely, G. R.; Moore, T. A.; Gust, D. *J. Am. Chem. Soc.* **1995**, *117*, 1657.
(42) Rohrer, M.; MacMillan, F.; Prisner, T. F.; Gardiner, A. T.; Mobius, K.; Lubitz, W. *J. Phys. Chem. B* **1998**, *102*, 4648.
(43) Bixon, M.; Jortner, J. *Adv. Chem. Phys* **1999**, *106*, 35.
(44) Bixon, M.; Jortner, J. *J. Phys. Chem.* **1986**, *90*, 3975.
(45) Altucci, C.; Borrelli, R.; De Lisio, C.; De Riccardis, F.; Persico, V.; Porzio, A.; Peluso, A. *Chem. Phys. Lett.* **2002**, *354*, 160.
(46) Pearl, G. M.; Zerner, M. C.; Broo, A.; McKelvey, J. *J. Comput. Chem.* **1998**, *19*, 781.
(47) Dewar, M. J. S.; Thiel., W. *J. Am. Chem. Soc.* **1977**, *99*, 4899.
(48) Stewart, J. J. P. *J. Comput. Chem.* **1989**, *10*, 210.
(49) Brookhaven Protein Databank, PDB entry 1AIG.
(50) Nabedryk, E.; Breton, J.; Okamura, M. Y.; Paddock, M. *Biochemistry* **2001**, *40*, 13286.
(51) Allen, J. P.; Feher, G.; Yeats, T. O.; Komiya, H.; Rees, C. *Proc. Natl. Acad. Sci. U. S. A.* **1985**, *85*, 8487.
(52) Debus, R. J.; Feher, G.; Okamura, M. Y. *Biochemistry* **1986**, *25*, 2279.
(53) Mulliken, R. S. *J. Am. Chem. Soc.* **1952**, *74*, 811.
(54) Hush, N. S. *Prog. Inorg. Chem.* **1967**, *8*, 391.
(55) Hush, N. S. *Electrochim. Acta* **1968**, *13*, 1005.
(56) Cave, R.; Newton, M. *Chem. Phys. Lett.* **1996**, *249*, 15.
(57) Creutz, C.; Newton, M. D.; Sutin, N. *J. Photochem. Photobiol. A: Chem.* **1994**, *82*, 47.
(58) Duschinsky, F. *Acta Phisicochim. URSS* **1937**, *7*, 551.
(59) Borrelli, R.; Peluso, A. *J. Chem. Phys.* **2003**, *119*, 8437.
(60) Del Re, G.; Förner, W.; Hofmann, D.; Ladik, J. *Chem. Phys.* **1989**, *139*, 265.
(61) Hopfield, J. J. *Proc. Natl. Acad. Sci. U. S. A.* **1974**, *71*, 3640.
(62) Villani, G. *J. Chem. Phys.* **2002**, *117*, 1279.
(63) Jang, S.; Cao, J. *J. Chem. Phys.* **2001**, *114*, 9959.
(64) De Schryver, F. C.; Declercq, D.; Depaemelaere, S.; Hermans, E.; Onkelinx, A.; Verhoven, J. W.; Gelan, J. *Photochem. Photobiol.* **1994**, *A82*, 171.
(65) Napper, A. M.; Read, I.; Waldeck, D. H. *J. Am. Chem. Soc.* **2000**, *122*, 5220.
(66) Balabin, I. A.; Onuchic, J. N. *Science* **2000**, *290*, 114.
(67) Graige, M. S.; Paddock, M. L.; Bruce, J. M.; Okamura, M. Y. *J. Am. Chem. Soc.* **1996**, *118*, 9005.
(68) Perkins, M. J. *Radical Chemistry*; Ellis Orwood, London: 1994.
(69) Siegbahn, P. E. M.; Blomberg, M. R. A.; Crabtree, R. H. *Theor. Chem. Acc.* **1997**, *97*, 289.
(70) Vermeglio, A.; Clayton, R. K. *Biochim. Biophys. Acta* **1977**, *461*, 159.
(71) Belloc, A. M.; Perchard, C.; Novak, A.; Josien, M. L. *J. Chim. Phys.* **1965**, *62*, 1344.
(72) Hasegawa, K.; Ono, T.; Noguchi, T. *J. Phys. Chem. B* **2000**, *104*, 4253.
(73) Schmidt, M. W.; Baldridge, K. K.; Boats, J.; Elbert, S. T.; Gordon, M. S.; Jensen, J. J.; Koseki, S.; Matsunaga, M.; Nguyen, K. A.; Su, S.; Windus, T. L.; Dupuis, M.; Montgomery, J. A. *J. Comput. Chem.* **1993**, *14*, 1347.
(74) Frisch, M. J.; Trucks, G. W.; Schlegel, H. B.; Gill, P. M. W.; Johnson, B. G.; Robb, M. A.; Cheeseman, J. R.; Keith, T.; Petersson, G. A.; Montgomery, J. A.; Raghavachari, K.; Al-Laham, M. A.; Zakrzewski, V. G.; Ortiz, J. V.; Foresman, J. B.; Cioslowski, J.; Stefanov, B. B.; Nanayakkara, A.; Challacombe, M.; Peng, C. Y.; Ayala, P. Y.; Chen, W.; Wong, M. W.; Andres, J. L.; Replogle, E. S.; Gomperts, R.; Martin, R. L.; Fox, D. J.; Binkley, J. S.; Defrees, D. J.; Baker, J.; Stewart, J. P.; Head-Gordon, M.; Gonzalez, C.; Pople, J. A. *Gaussian 94*, revision C.2; Gaussian, Inc.: Pittsburgh, PA, 1995.
(75) Stewart, J. J. P. *MOPAC7*, Quantum Chemistry Program Exchange.
(76) Hohenberg, P.; Khon, W. *Phys. Rev.* **1964**, *136*, B864.
(77) Khon, W.; Sham, J. *Phys. Rev.* **1965**, *140*, A1133.
(78) Dewar, M. J. S.; McKee, M. L.; Rzepa, H. S. *J. Am. Chem. Soc.* **1978**, *100*, 3607.
(79) Lee, C.; Yang, W.; Parr, R. G. *Phys. Rev. B* **1988**, *37*, 785.
(80) Hay, P. J.; Wadt, W. R. *J. Chem. Phys.* **1985**, *82*, 270.
(81) Hay, P. J.; Wadt, W. R. *J. Chem. Phys.* **1985**, *82*, 284.
(82) Hay, P. J.; Wadt, W. R. *J. Chem. Phys.* **1985**, *82*, 299.
(83) Dunning, T. H. *J. Chem. Phys.* **1971**, *55*, 716.
(84) Rienstra-Kirakofe, J. C.; Tschumper, G. S.; Schaefer, H. F., III; Nandi, S.; Ellison, G. B. *Chem. Rev.* **2002**, *102*, 231.
(85) Park, J. T.; Light, J. C. *J. Chem. Phys.* **1986**, *85*, 5870.
(86) Hamilton, P.; Light, J. C. *J. Chem. Phys.* **1986**, *84*, 306.
(87) Bacic, Z.; Light, J. C. *J. Chem. Phys.* **1986**, *85*, 4594.
(88) Peluso, A.; Santoro, F.; Del Re, G. *Int. J. Quantum Chem.* **1997**, *63*, 233.
(89) Package available free of charge via Internet at http://pcdual-.chem.unisa.it.